SINTEK JURNAL: Jurnal Ilmiah Teknik Mesin
ISSN: 2088-9038, e-ISSN: 2549-9645
Homepage: http://jurnal.umj.ac.id/index.php/sintek

LATTICE STRAIN ANALYSIS OF TITANIUM ROD PROCESSED BY EQUAL-CHANNEL ANGULAR PRESSING (ECAP) WITH BC ROUTE USING X-RAY DIFFRACTION LINE BROADENING ANALYSIS

Ibrahim Purawiardi[1,*], I Nyoman Gede Putrayasa Astawa[1]
[1]Research Centre for Metallurgy and Materials, Indonesian Institute of Sciences (LIPI),
National Science Technopark (PUSPIPTEK) Bld. 470, South Tangerang 15314, Indonesia

*E-mail: ibrahimpurawiardi@gmail.com

Accepted: 18-02-2021 Revised: 08-05-2021 Approved: 01-06-2021

ABSTRACT

Equal-channel angular pressing (ECAP) was one of severe plastic deformation method in order to increase the mechanical properties of solid metal without changing its dimension and without adding any alloy elements. The change of mechanical properties on ECAPed metals was caused by the change of lattice strain, so that the lattice strain investigation was recommended for evaluating ECAPed metals. In this study, pure titanium rod was treated by ECAP with Bc route and two passes. Before ECAPed, this titanium rod consisted of two lattice strains i.e. 0.001014 and 0.005241. After ECAPed, a lattice strain of 0.005241 reduces to 0.003205 and 0.003555 after first pass and reduces again to 0.002576 and 0.002647 after two passes. Meanwhile, a lattice strain of 0.001014 was annihilated after ECAP treatment. These results show that ECAP treatment can reduce and eliminate lattice strains on titanium rod. This study also shows that the reduction of lattice strains implicates to the increasing of its hardness value.

Keywords: titanium rod, ECAP, line broadening, lattice strain, hardness.

1. INTRODUCTION

The severe plastic deformation (SPD) method is an effective way in order to improve the mechanical properties of pure titanium metal without adding any alloy elements and without changing its diameter [1].

One of some SPD methods that can be applied to pure titanium rod is equal-channel angular pressing (ECAP) [2]. The working principle of ECAP is that a solid metal in the form of a cylinder (rod) is passed through a cylindrical channel with a certain angle while being pressed forcefully with a certain load [3]. The illustration of this process can be seen in Figure 1.a. With this treatment process, it is hoped that the atomic compaction will be occurred so that it can implicate to improve the mechanical properties of pure titanium rod, especially in its hardness value.

Several studies on the application of ECAP to titanium rods have been published. In general, research only discusses the effect of ECAP treatment including route and the number of passes on improving its mechanical properties. The cause of the increasing of mechanical properties due to ECAP which is generally discussed is only focused in the change of grain to become smaller and more uniform. [2]. However, it is rare to discuss the change in residual stress during ECAP process. It is because the residual stress is very difficult to

be determined quantifiably. However, the residual stress can still be predicted by the presence of residual strain. The residual strain can be detected by the presence of lattice strain. And, the lattice strain can determined by means of x-ray diffraction (XRD) analytical method [4].

Therefore, this study tries to determine the cause of the increasing of mechanical properties (i.e. hardness value) of titanium rods due to ECAP treatment from the lattice strain point of view, which this study is rarely conducted. Furthermore, in order to perform lattice strain analysis, a special analytical method is used, i.e. Williamson-Hall plot method.

Williamson-Hall Plot Method

The Williamson-Hall plot method is commonly used for analyzing the x-ray diffraction line broadening [5-12].

The principle of this method on solid metal sample is that the line broadening of x-ray diffraction peak (*B*, in radian) is effected by lattice strain. This principle is then formulated in an equation below [12]

$$B = 4\varepsilon \tan\theta \quad (1)$$

$$B\,Cos\,\theta = 4\varepsilon\,Sin\,\theta \quad (2)$$

where ε is lattice strain and θ is diffraction angle (degree). Equation (2) is then thought as a linear equation of $y = ax$ where y is $B\,Cos\,\theta$, x is $4\,Sin\,\theta$, and a or gradient is ε . For making the analysis easier to perform, a Williamson-Hall plot can then be made where x-axes (abscissa) is $4\,Sin\,\theta$ and y-axes (ordinate) is $B\,Cos\,\theta$. Thus, with this Williamson-Hall plot, the value of lattice strain (ε) can be obtained as a gradient value of the linear regression line equation.

However, in practice it is rare to find an ideal linear regression line equation ($y = ax$). The equation that is often found is $y = ax + b$, where b is an intersection point of the ordinate. However, the $y = ax + b$ equation can be tolerated and considered as $y = ax$ provided that the value of the b intercept is very close to zero. In the calculation, the line broadening of diffraction peak (*B*) is calculated from the value of the full width at half maximum (FWHM), where its value in $^o2\theta$ unit is then converted into radian (rad) unit.

2. METHODS

The samples were three solid titanium rods (Ti rods) with a diameter of 13.5 mm and a length of 65 mm. The first sample was not given ECAP treatment. The second sample was ECAPed with Bc route for one pass. The third sample was ECAPed with Bc route for two passes. The mechanism of ECAP with Bc route can be seen in Figure 1.

These samples were then characterized by a Brüker x-ray diffractometer (XRD) with Co-Kα tube (λ = 1.78901 Å). The range of 2θ used is 30^o to 120^o. After being characterized by XRD, the value of 2θ and FWHM were calculated using *Highscore Plus* (HSP) software. After that, these samples were analyzed for lattice strain using the Williamson-Hall method.

Then, these samples were measured for their Brinell hardness (HB) values using AFFRI hardness tester equipment with a compressive load of 187.3 kgf.

3. RESULTS AND DISCUSSION

An XRD characterization results in the form of diffraction patterns of samples can be seen in Figure 2 and Figure 3. Then, for making line broadening analysis become easier, each diffraction peak is assigned a peak number (see Figure 2). Then, the diffraction peaks are calculated for determining 2θ and FWHM values where the calculation results can be seen in Table 1.

3.1. Plot of FWHM vs 2θ

For analyzing the lattice strains, the first step that needs to be done is to sort out the diffraction peaks indicated that there is a contribution to the effect of lattice strain in the broadening of diffraction peaks. To sort them out, a plot of FWHM as a function of 2θ can be

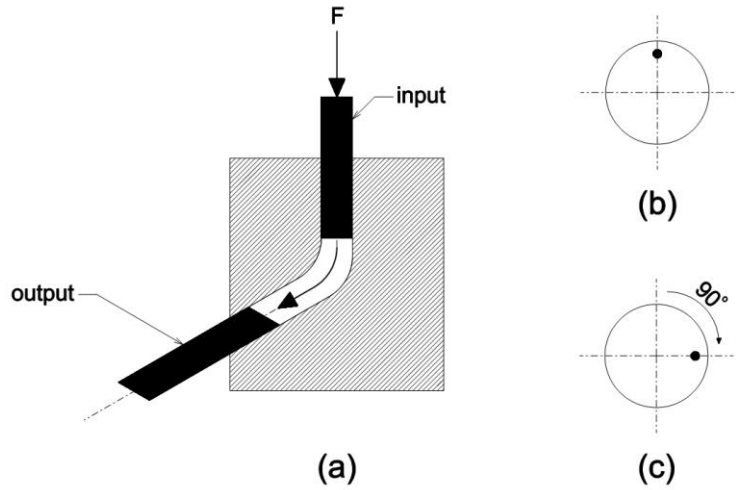

Figure 1. (a) Mechanism of Bc route ECAP with 120° of elbow in this study. (b) Top view of sample position for first pass. (c) Top view of sample position for second pass.

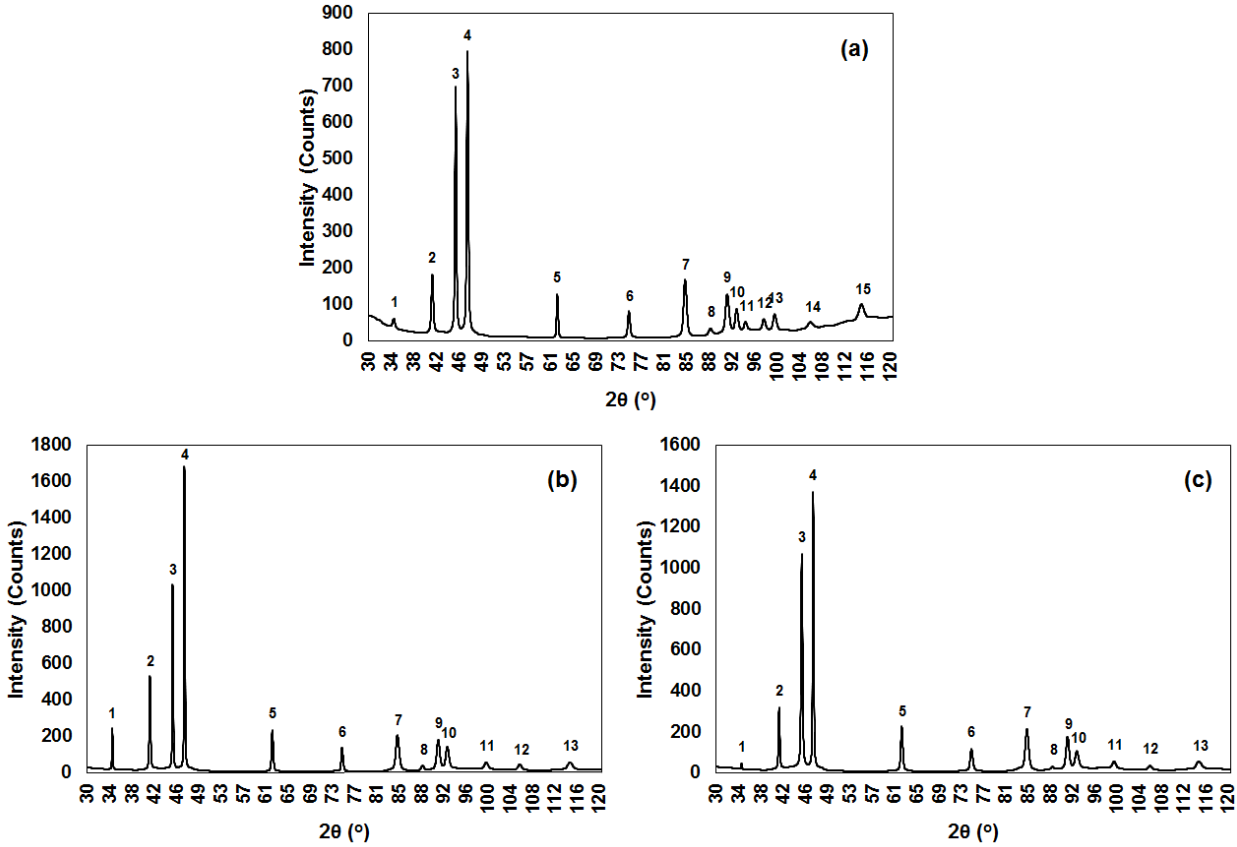

Figure 2. Diffraction patterns of titanium rod samples with diffraction peak numbers. (a) Before ECAP. (b) After first pass of ECAP. (c) After second pass of ECAP.

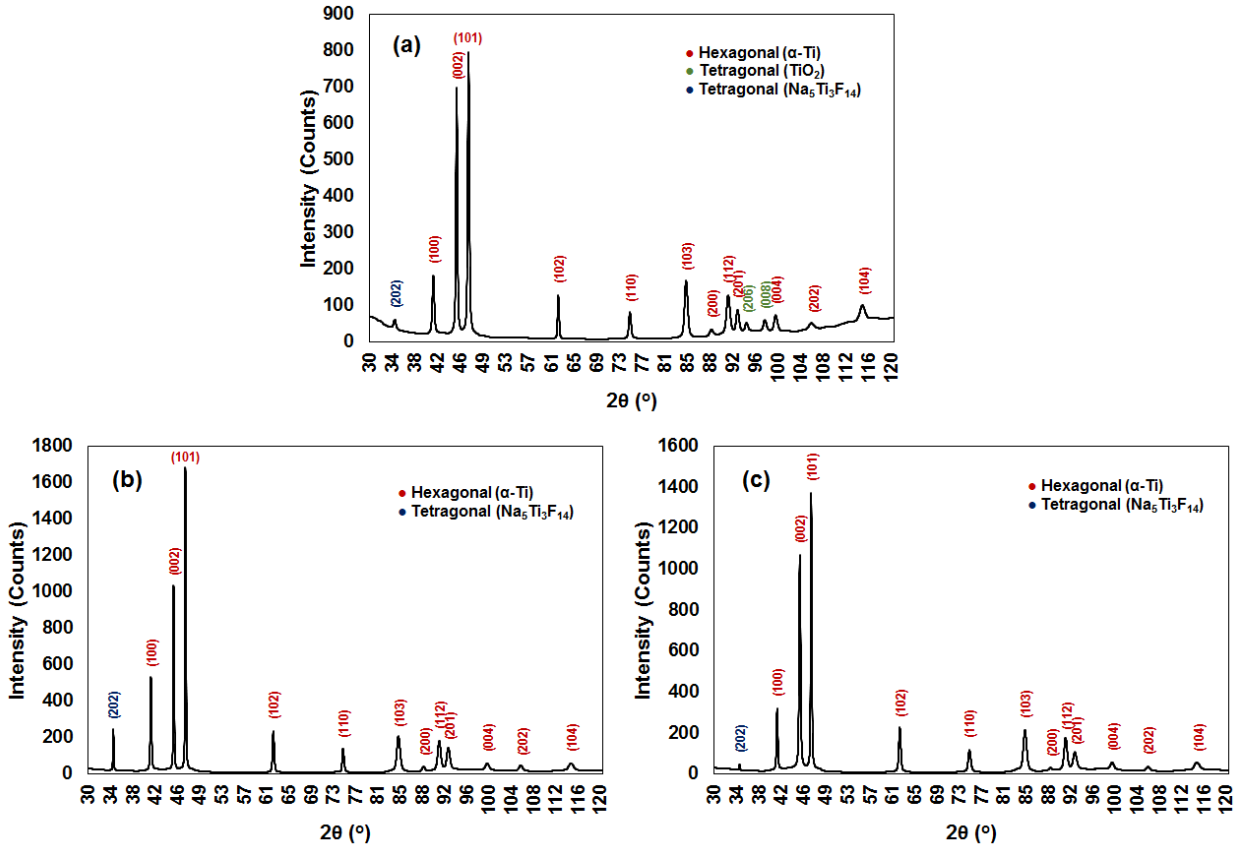

Figure 3. Diffraction peaks of titanium rod samples with the indexing of Miller indices and phases. (a) Before ECAP. (b) After first pass of ECAP. (c) After second pass of ECAP.

Table 1. Diffraction peak numbers, 2θ and FWHM of samples.

Diffraction Peak No.	Before ECAP		1 Pass of ECAP		2 Passes of ECAP	
	2θ (°)	FWHM (°2θ)	2θ (°)	FWHM (°2θ)	2θ (°)	FWHM (°2θ)
1	34.3127	0.4487	34.3449	0.1309	34.4112	0.1122
2	40.9306	0.3739	40.9263	0.2057	40.9704	0.2244
3	44.9283	0.2617	44.9013	0.1309	44.9267	0.2617
4	46.9660	0.2991	46.9724	0.1309	46.9322	0.1683
5	62.3689	0.2244	62.3334	0.2617	62.4146	0.3365
6	74.6463	0.3739	74.5355	0.2617	74.6053	0.4487
7	84.2720	0.5235	84.2150	0.5983	84.3071	0.5983
8	88.6241	0.5983	88.5781	0.5235	88.7407	0.5983
9	91.4863	0.5983	91.3344	0.5235	91.4090	0.5235
10	93.0962	0.4487	92.9280	0.5235	93.0282	0.5983
11	94.6376	0.4487	99.7265	0.5983	99.5506	0.5983
12	97.7893	0.4487	105.5693	0.5983	105.8535	0.5983
13	99.6379	0.5235	114.3767	0.8974	114.3400	0.8974
14	105.7398	0.8974				
15	114.4701	0.8974				

Table 2. Brinell hardness (HB) testing results.

Pass	Repetition			Average HB
	1	2	3	
0	158.50	157.00	153.20	156.23
1	220.00	252.00	233.00	235.00
2	250.80	252.00	253.30	252.03

used [4]. Theoretically, if there is an effect of lattice strain in the broadening of diffraction peaks, a linear line will be formed with a positive gradient (slope) in the 2θ range of 0^o - 100^o [4]. Therefore, the FWHM vs 2θ plot in this study was also observed in this range as well (see Figure 4). With the limitation of observation (i.e. $2\theta = 0^o$ - 100^o), in each sample there are two diffraction peaks that are not observed, i.e. diffraction peaks number 14 and 15 in first sample (before ECAP) and diffraction peaks number 12 and 13 in the two ECAPed samples.

According to the linear regression lines formed in Figure 4, the probability of the effect of lattice strain on the sample before ECAP is at the diffraction peaks number 3, 6, 7, 8, 9, 10 and 13 (see Figure 4.a). So it can be ascertained that there was no lattice strain effect on the line broadening at the diffraction peaks number 1, 2, 4, 5, 11 and 12. While in the ECAPed samples with one pass, the probability of the effect of lattice strain was found at the diffraction peaks number 1, 2, 3, 4, 5, 7, 8, 9, 10 and 11, as well as only diffraction peak number 6 which has no lattice strain effect (see Figure 4.b). Whereas in the 2-pass ECAPed sample, the effect of lattice strain was probably found on all observed diffraction peaks (see Figure 4.c).

The decrease in the number of diffraction peaks that did not have the effect of lattice strain after ECAP indicated a more even lattice strain distribution probability after ECAP treatment. However, to prove it, the diffraction peaks that contribute to the formation of the linear regression lines in Figure 4 must then be plotted in the Williamson-Hall plot.

3.2. Williamson-Hall Plot

The Williamson-Hall plots on diffraction peaks that have a probability of the effect of lattice strains based on the previous results in Figure 4 can be seen in Figure 5. Two linear regression lines are formed in Figure 5.a, Figure 5.b and Figure 5.c. In these Williamson-Hall plots, the gradient values (or slopes) of the linear regression lines represent the values of the lattice strains. Thus, based on the analysis of the Williamson-Hall plots show that the calculated lattice strains (ε) obtained are ε_1 = 0.001014 and ε_2 = 0.005241 for a sample before ECAP, ε_1 = 0.003205 and ε_2 = 0.003555 for 1-pass ECAPed sample as well as ε_1 = 0.002576 and ε_2 = 0.002647 for 2-pass ECAPed sample. These results are also presented in the form of a bar graph in Figure 6.a.

If the change of the lattice strain value (ε) is observed to the number of passes of the ECAP treatment, the lattice strain values in the samples after ECAP are the decreasing of one of the lattice strain value before ECAP, i.e. ε_2 = 0.005241. This is evidenced by the exponential regression curve formed in Figure 6.b where the correlation shows R^2 which is very close to 1, i.e. 0.9535. This shows that the ECAP treatment process on titanium rods is proven to reduce the value of lattice strain. Meanwhile, one of the lattice strain value of unECAPed sample (i.e. ε_1 = 0.001014) did not contribute at all to the curve in Figure 6.b. It shows that ε_1 = 0.001014 is eliminated after ECAPed. This indicates a strong suspicion that in addition to a decrease in a value of the lattice strain, the ECAP treatment on titanium rods can also remove a small value of lattice strain. Basically, the low lattice strain value of ε1 = 0.001014 also decreased after 1-pass ECAP treatment, where it decreased from ε1 = 0.001014 to ε1 = 0. Thus, theoretically, a ε2 = 0.005241 of unECAPed sample can also be eliminated to ε2 = 0 by increasing the number of passes. However, this could not be done because when 3-pass ECAP was applied, the

sample was damaged (broken and cracked). So that the ECAP treatment with Bc route on titanium rod samples was only effective until 2 passes.

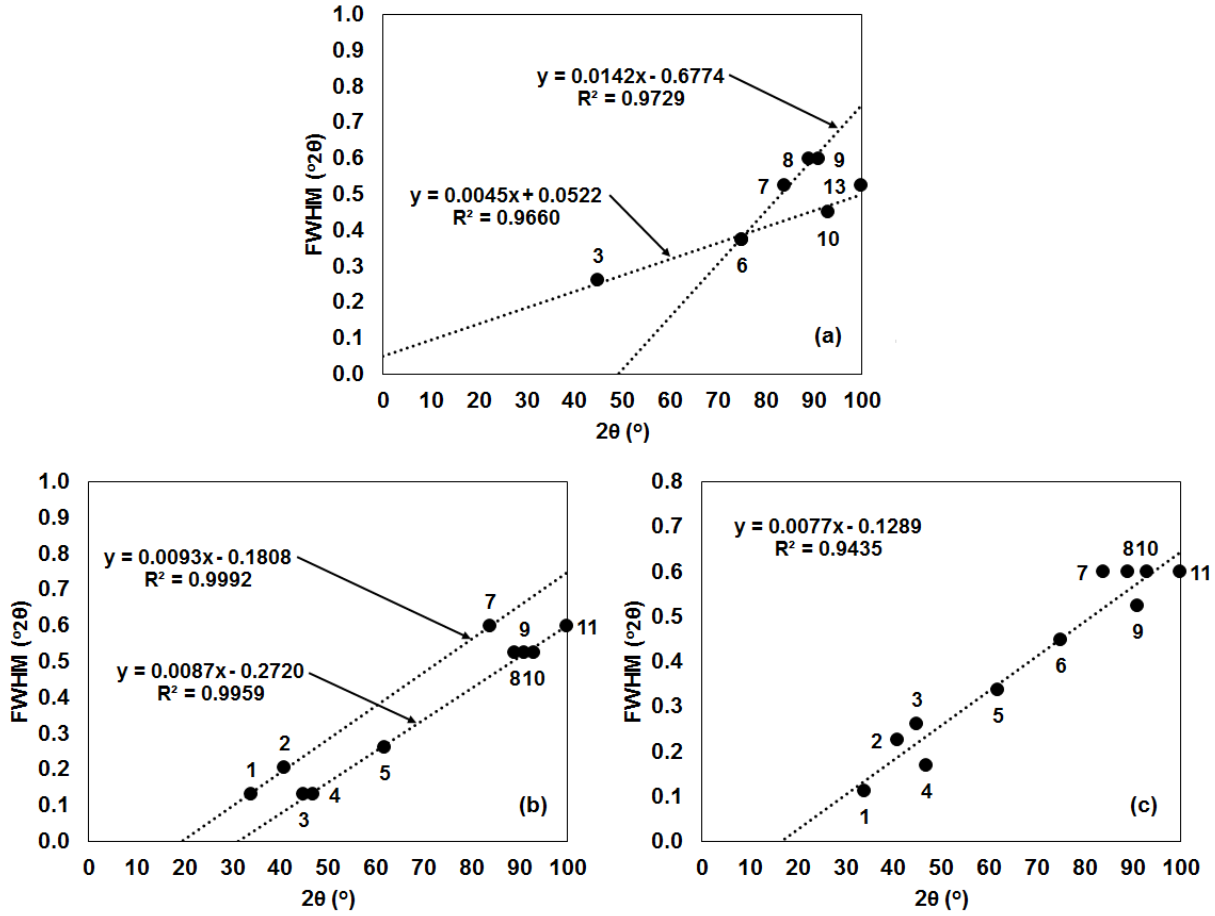

Figure 4. FWHM vs 2θ plots of titanium rod samples. (a) Before ECAP. (b) After first pass of ECAP. (c) After second pass of ECAP.

Lattice Strain-Hardness Relationship

The decrease of the lattice strain value on the titanium rod as a result of the ECAP treatment that is occurred (see Figure 6.b) led to suspicion of the implications for the changes in its mechanical properties. To prove this, the decrease of the lattice strain value that occurs is correlated with the changes of mechanical properties. In this study, the mechanical properties tested were the hardness values on the Brinell scale (HB). The results of the Brinell hardness tests are shown in Table 2. The average hardness (HB) values were then used in the analysis of the lattice strain-hardness relationship.

The plot of the hardness value (HB) as a function of lattice strain value (ε) is shown in Figure 7. The linear regression line formed in Figure 7 shows that the relationship between them is linear relationship. Based on its linear regression line, it can be seen that the smaller the lattice strain value, the greater the Brinell hardness value. That is, the decrease in the lattice strain value on the titanium rod resulted from ECAP treatment implicates to the increasing of Brinell hardness value.

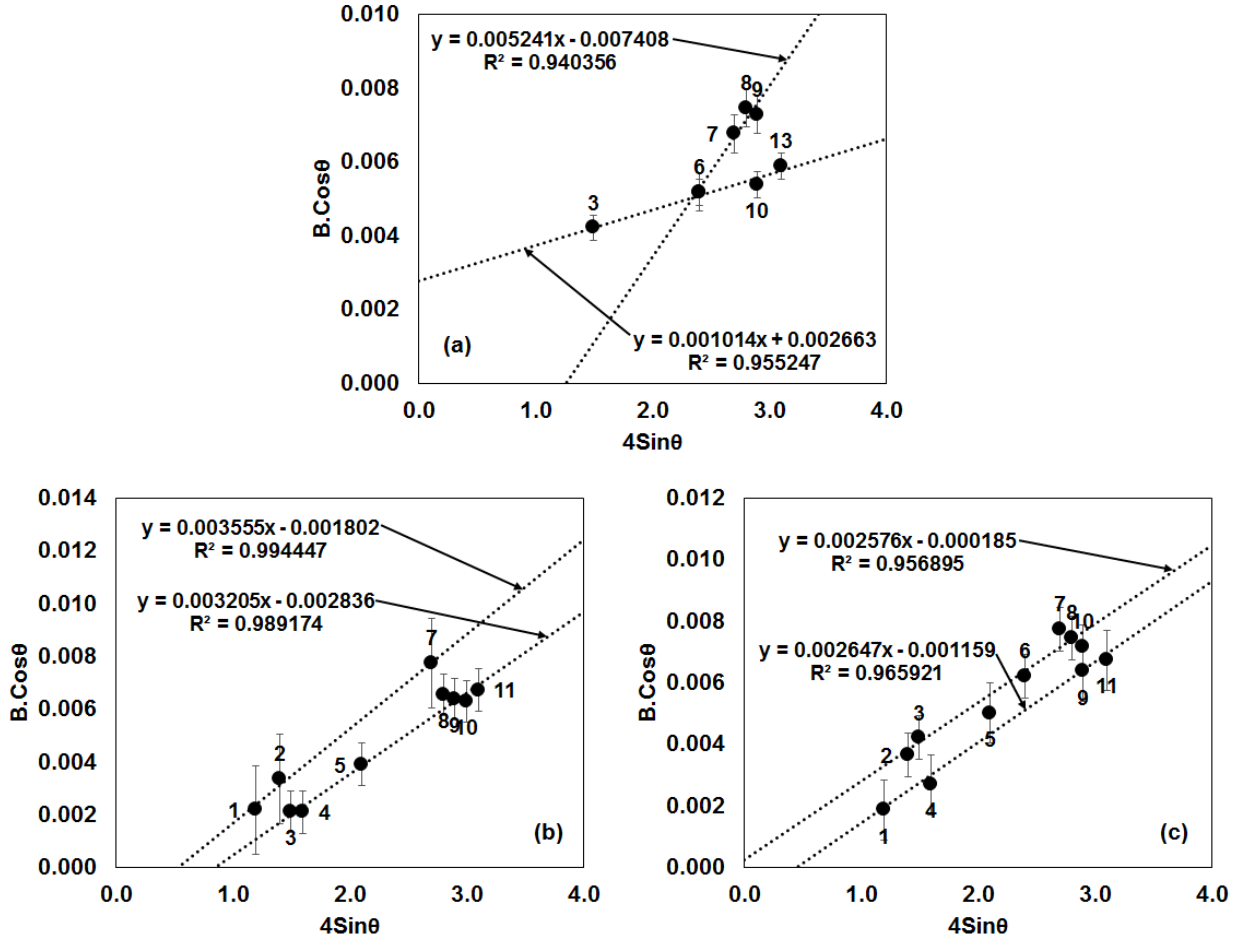

Figure 5. Williamson-Hall plots of titanium rod samples. (a) Before ECAP. (b) After first pass of ECAP. (c) After second pass of ECAP. Error bars indicate 1x standard deviation.

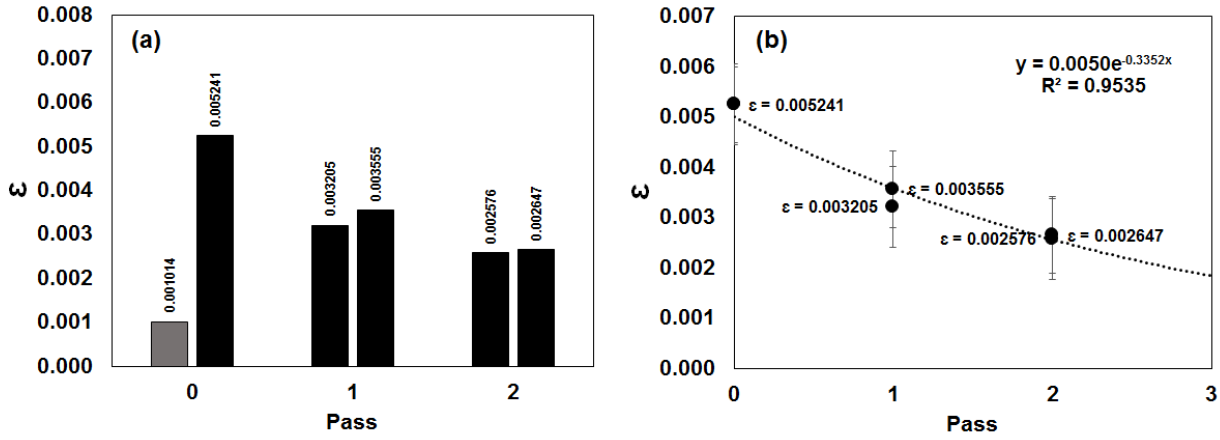

Figure 6. Graph of lattice strain (ε) vs pass. (a) A bar graph. (b) An exponential regression curve with lattice strain (ε) as a function of pass. Error bars indicate 1x standard deviation.

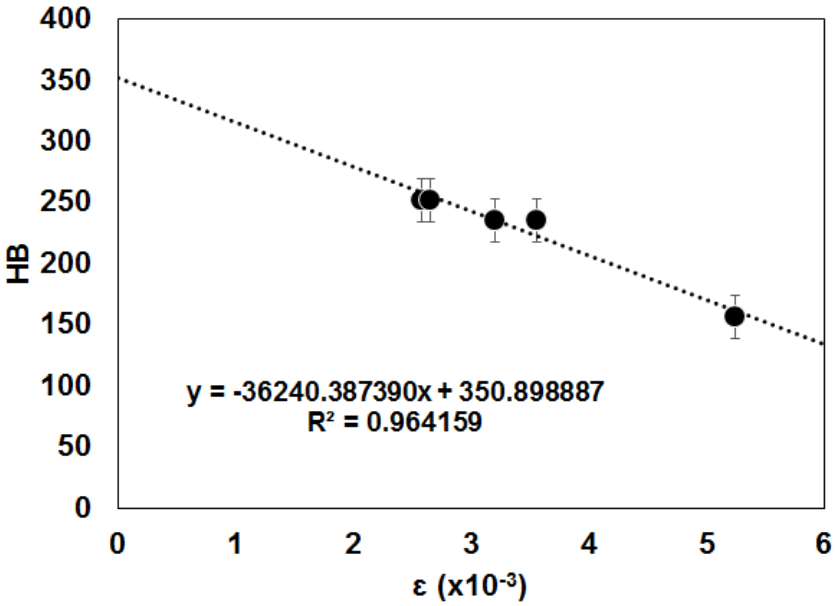

Figure 7. Linear regression line with its equation that shows Brinell hardness (HB) as a function of lattice strain (ε). Error bars indicate 1x standard deviation.

Therefore, it is found that the ECAP treatment on titanium rods is fairly effective method to increase its hardness value.

Lattice Strain Distribution on Ti Rods

In Figure 3, there are diffraction peaks which are signed as number 1. These diffraction peaks tend to be $Na_5Ti_3F_{14}$ phase with (202) planes of tetragonal crystal structures. These phases are commonly used as coating layer on titanium to prevent the formation of TiO_2 layer [13].

In the unECAPed titanium rod sample, the $Na_5Ti_3F_{14}$ phase did not contributed to the detected lattice strain value (see Figure 5.a). Whereas in the ECAPed titanium rod samples, this phase contributed to the lattice strain values of $\varepsilon_2 = 0.003555$ (see no. 1 in Figure 5.b) and $\varepsilon_2 = 0.002647$ (see no. 1 in Figure 5.c). Uniquely, both of these ε_2 values are greater than their ε_1 values (0.003205 and 0.002576). This shows that the lattice strain values are higher in the area where the $Na_5Ti_3F_{14}$ coatings are formed.

Generally, the $Na_5Ti_{13}F_{14}$ coating layer is on the outer side of the titanium rod. So it can be strongly assumed that the lattice strain value on the outer side of the titanium rod is higher than on the inside. And, with this assumption, it can also be assumed that the hardness value on the outer side of titanium rod is lower than on the inside. If the direction of the lattice strain vector is considered to be entirely in the longitudinal direction, then the illustration of the lattice strain distribution can be depicted as in Figure 8.a, Figure 8.b and Figure 8.c.

In the unECAPed sample, there is a lattice strain value of $\varepsilon_1 = 0.001014$. This value is difficult to be described as a distributed vector on the titanium rod sample. However, its direction can still be predicted even though the probability is very low. If we consider that the lattice strain of $\varepsilon_2 = 0.005241$ is in the longitudinal axes position and its direction is considered as a main vector while $\varepsilon_1 = 0.001014$ is considered as a projection vector, then these two vectors will be separated by an angle (θ_P) of 78.84°. So that the illustration of the lattice strain distribution directions can be depicted as in Figure 8.d, respectively.

CONCLUSION

Based on the results of this study, there are three advantages obtained from Bc route ECAP treatment on pure titanium rods, i.e. reducing the lattice strain value, eliminating small lattice strain value and increasing the hardness value.

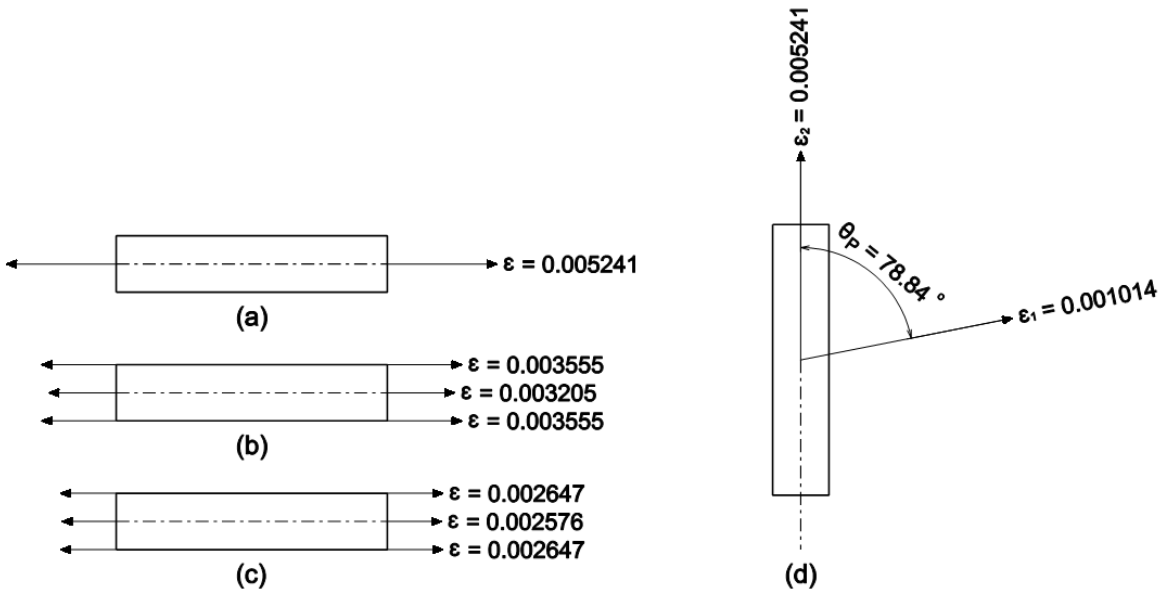

Figure 8. Predicted lattice strain distribution on titanium rod samples. (a) A lattice strain Before ECAP. (b) Lattice strains after first pass of ECAP. (c) Lattice strains after second pass of ECAP. (d) Two predicted lattice strains before ECAP.

After being treated by Bc route ECAP treatment, the distribution of the lattice strain values tended to be more evenly distributed with a decreasing in their values, where on the outer side was higher that on the inside of titanium rods.

The decrease of the remaining lattice strain value on titanium rod after being ECAPed effects an increase in the hardness value.

ACKNOWLEDGEMENT

Special thanks to Mr. Arda Yogatama from P.T. Multiteknindo Infotronika for the facility of HSP software.

REFERENCES

[1] Kardashev, B. K., Narykova, M. V., Betekhtin, V. I., Kadomtsev, A. G. Evolution of Elastic Properties of Ti and its Alloys due to Severe Plastic Deformation. Physical Mesomechanics. 2020; 23: 193-198. doi: 10.1134/S1029959920030029.

[2] Semenova, I. P., Polyakov, A. V., Raab, G. I., Lowe, T. C., Valiev, R. Z. Enhanced Fatigue Properties of Ultrafine-Grained Ti Rods Processed by ECAP-conform. Journal of Materials Science. 2012; 47: 7777-7781. doi: 10.1007/s10853-012-6675-9.

[3] Manjunath, G. K., Udaya Bhat, K., Preetham Kumar, G. V., Ramesh, M. R. Microstructure and Wear Performance of ECAP Processed Cast Al-Zn-Mg Alloys. Transactions of the Indian Institute of Metals. 2018; 71: 1919-1931. doi: 10.1007/s12666-018-1328-6.

[4] Suryanarayana, C. and Grant Norton, M. 1998. *X-ray Diffraction: a Practical Approach*. New York, New York: Plenum Press.

[5] Dey, P. C., Das, R. Impact of Silver Doping on the Crystalline Size and Intrinsic Strain of MPA-Capped CdTe Nanocrystals: a Study by Williamson-Hall Method and Size-Strain Plot Method. Journal of Materials Engineering and Performance. 2021. doi: 10.1007/s11665-020-05358-9.

[6] Erdogan, E. X-ray Line Broadening Study on Sputtered InGaN Semiconductor with Evaluation of Williamson-Hall and Size-Strain Plot Methods. Indian Journal of Physics. 2019; 93: 1313-1318. doi: 10.1007/s12648-019-01403-z.

[7] Islam, S. A. U., Ikram, M. Structural Stability Improvement, Williamson Hall Analysis and Band-gap Tailoring through A-site Sr Doping in Rare Earth Based Double Perovskite La_2NiMnO_6. Rare Metals. 2019; 38: 805-813. doi: 10.1007/s12598-019-01207-4.

[8] Kulkarni, A. B., Mathad, S. N. Synthesis and Structural Analysis of Co-Zn-Cd Ferrite by

Williamson-Hall and Size-Strain Plot Methods. International Journal of Self-Propagating High-Temperature Synthesis. 2018; 27: 37-43. doi: 10.3103/S10613862180 1003X.
[9] Madhavi, J. Comparison of Average Crystallite Size by X-ray Peak Broadening and Williamson-Hall and Size-Strain Plots for VO^{2+} Doped ZnS/CdS Composite Nanopowder. SN Applied Sciences. 2019; 1: 1509. doi: 10.1007/s42452-019-1291-9.
[10] Norouzzadeh, P., Mabhouti, K., Golzan, M. M., Naderali, R. Consequence of Mn and Ni Doping on Structural, Optical and Magnetic Characteristics of ZnO Nanopowders: the Williamson-Hall Method, the Kramers-Kronig Approach and Magnetic Interactions. Applied Physics A. 2020; 126: 154. doi: 10.1007/s00339-020-3335-9.
[11] Pushkarev, S. S., Grekhov, M. M., Zenchenko, N. V. X-ray Diffraction Analysis of Features of the Crystal Structure of GaN/$Al_{0.32}Ga_{0.68}N$ HEMT-Heterostructures by the Williamson-Hall Method. Semiconductors. 2018; 52: 734-738. doi: 10.1134/S1063782618060209.
[12] Kafashan, H. X-ray Diffraction Line Profile Analysis of Undoped and Se-Doped SnS Thin Films Using Scherrer's, Williamson-Hall and Size-Strain Plot Methods. Journal of Electronic Materials. 2018; 48: 1294-1309. doi: 10.1007/s11664-018-6791-7.
[13] Vajo, J. J., Adjorlolo, A. A., Graetz, J. Titanium-based Coatings and Methods for Making Coatings. EP3677705A2 (Patent). 2020.